Published in final edited form as:
Bioconjug Chem. 2011 April 20; 22(4): 777–784. doi:10.1021/bc100584d.

Near-infrared pH-activatable Fluorescent Probes for Imaging Primary and Metastatic Breast Tumors

Hyeran Lee, **Walter Akers**, **Kumar Bhushan**, **Sharon Bloch**, **Gail Sudlow**, **Rui Tang**, and **Samuel Achilefu***
Department of Radiology, Washington University, St. Louis, Missouri 63110

Abstract

Highly tumor selective near-infrared (NIR) pH-activatable probe was developed by conjugating pH-sensitive cyanine dye to a cyclic Arginine-Glycine-Aspartic acid (cRGD) peptide targeting $\alpha_v\beta_3$ integrin (ABIR), a protein that is highly overexpressed in endothelial cells during tumor angiogenesis. The NIR pH-sensitive dye used to construct the probe exhibit high spectral sensitivity with pH changes. It has negligible fluorescence above pH 6 but becomes highly fluorescent below pH 5, with a pKa of 4.7. This probe is ideal for imaging acidic cell organelles such as tumor lysosomes or late endosomes. Cell microscopy data demonstrate that binding of the cRGD probe to ABIR facilitated the endocytosis-mediated lysosomal accumulation and subsequent fluorescence enhancement of the NIR pH-activatable dye in tumor cells (MDA-MB-435 and 4T1/*luc*). A similar fluorescence enhancement mechanism was observed in vivo, where the tumors were evident within 4 h post injection. Moreover, lung metastases were also visualized in an orthotopic tumor mouse model using this probe, which was further confirmed by histologic analysis. These results demonstrate the potential of using the new integrin-targeted pH-sensitive probe for the detection of primary and metastatic cancer.

INTRODUCTION

Optical molecular imaging often utilizes activatable probes where fluorescence signal can be amplified by selective molecular events. These include the use of enzyme activity (1–8), pH (9–12), or the presence of reactive oxygen/nitrogen species (13) to visualize specific biological processes associated with the disease state. In particular, tumor-related enzyme activatable probes are widely used to visualize tumor biomarkers in vivo (14–21). However, most tumor biomarkers are also a part of normal physiological processes and thus imaging sensitivity and specificity are hampered by high background signal from the non-target tissues. Other tumor hallmarks such as acidosis and hypoxia have been explored as alternative approaches to enzyme-mediated imaging strategy to improve signal-to-background ratio. Acidosis has been an attractive target for tumor imaging (22) and this strategy is based on the underlying principle that the tumor's extracellular metabolic microenvironment is relatively acidic because of the activated Na^+/H^+ exchanger (NHE1) and the H^+/lactate co-transporter systems in cancer cells (23). However, there remains a challenge to design a probe targeting acidic tumor features. First, tumor cells have acidic interstitial extracellular pH (pHe, 6.2–6.9) rather than acidic intracellular pH (pHi) with a small pH difference from normal cells (7.3–6.4) (23). Second, the pKa of the fluorescent probe has to match the acidic extracellular tumor pH. To overcome these challenges, Urano et. al. recently developed pH-activatable BODIPY dyes that target the human epidermal

*Corresponding Author: Samuel Achilefu, Ph.D, Department of Radiology, Washington University School of Medicine, 4525 Scott Avenue, St. Louis, MO 63110, Tel: 314-362-8599, achilefus@mir.wustl.edu.

growth factor receptor type 2 (HER2) for tumor imaging ex vivo (11). The report demonstrated the potential of using pH-activatable dyes for tumor imaging with improved specificity by targeting acidic tumor organelles while minimizing signals from non-target tissue. However, BODIPY dyes exhibit absorption maxima in the visible region where tissue penetration of light is shallow and thus less optimal for noninvasive in vivo imaging. Therefore, near-infrared (NIR) imaging probes are essential for deep tissue light penetration and low autofluorescence. In particular, NIR fluorescent probes that respond to pH changes within physiologically relevant range would enhance tumor imaging while minimizing the background fluorescence.

With this goal in mind, we employed two complementary strategies to improve tumor targeting sensitivity and specificity of a NIR pH activatable probe: 1) conjugation of a pH-sensitive NIR dye to $\alpha_v\beta_3$ integrin receptor (ABIR)-avid peptide, cRGD, to promote selective accumulation of the probe in tumor cells and tissue; and 2) fluorescence amplification in the highly acidic lysosomes of tumor cells while minimizing fluorescence from non-target tissues. RGD peptides have been shown to exhibit high binding affinity for ABIR that are up-regulated in tumor cells (24–27). In addition, the new fluorescent probe is silent in the NIR window at pH > 5 but highly fluorescent in the acidic environment (pH < 5), with a pKa value of 4.7 that closely matches lysosomal pH (Figure 1). We explored the probe's versatility as an imaging probe to detect primary and metastatic breast tumors in both subcutaneous and orthotopic mouse models.

MATERIALS AND METHODS

General

All chemicals were purchased from commercial sources and were used without further purification. The starting indole, sodium (2,3,3-trimethyl-*3H*-indole-5-yl)sulfonate (**2**) and Vilsmeier-Haack reagents **3** and **5** were prepared according to published procedures (28,29). ^{1}H NMR data were recorded on a 300 MHz spectrometer at ambient temperature in DMSO-d_6 and referenced to tetramethylsilane (TMS) as an internal standard. High resolution mass spectra (HR-MS) were recorded on a hybrid linear ion trap-Fourier transform mass Spectrometer.

Synthesis of pH-activatable dye 1

A mixture of the indole intermediate **2** (100 mg, mmol) and Vilsmeier-Haack reagent **3** (90 mg, mmol) were heated under reflux in the presence of sodium acetate (55 mg, 0.67 mmol) in 10 mL mixed solutions of CH_3CN/H_2O (95%/5%, v/v) for 20 h. After cooling, 5% of HCl in H_2O was added to the resultant mixture. MeOH was then added after the removal of H_2O and the crude material was subjected to reverse-phase C-18 column chromatography eluting CH_3CN/H_2O to afford 46 mg of the desired dye. Yield 76%. ^{1}H NMR (300 MHz, DMSO-d_6) δ 1.47 (s, 12 H), 1.80 (m, 2H), 2.62 (m, 4H), 6.14 (br d, *J* = 14 Hz, 2H), 7.17 (d, *J* = 8 Hz, 2H), 7.61 (d, *J* = 8 Hz, 2H), 7.72 (s, 2H), 8.25 (br d, *J* = 14 Hz, 2H). NIR/vis: λ_{abs}= 778 nm, λ_{em} = 791 nm, ε = 1.4 × 10^5 $M^{-1}cm^{-1}$ (pH < 5), λ_{abs}= 516 nm (pH > 5), pKa = 4.7. Φ_F (MeOH): 0.036. ESI-MS, *m/z*: 615 (M^+ -Na + H, 100%).

Meso-carboxy functionalized dye 4

To a solution of sodium [1-(4′-sulfonatobutyl)-2,3,3-trimethyl-*3H*-indolium]-5-sulfonate (**2**, 45 mg, 0.17 mmol) was added Vilsmeier-Haack reagent **5** (35 mg, 0.086 mmol) in 10 mL mixed solutions of EtOH/acetic anhydride (1:1, v/v) in the presence of sodium acetate (14 mg, 0.17 mmol). This solution was then heated under reflux for 24 h. The reaction progress was monitored by UV/vis and LC-MS until starting materials **2** and **3** were almost consumed and the dye **4** was formed as the major product. After cooling, the crude material was

subjected to reverse-phase C-18 column chromatography eluting with CH_3CN/H_2O to afford 11 mg of green dye powder. Yield 18%. ^{1}H NMR (300 MHz, DMSO-d_6)) δ 1.26 (s, 12 H), 1.90 (m, 2H), 2.60 (m, 4H), 6.09 (br d, *J* = 14 Hz, 2H), 6.96 (br d, *J* = 14 Hz, 2H), 7.04 (d, *J* = 8 Hz, 2H), 7.34 (d, *J* = 8 Hz, 2H), 7.52 (d, *J* = 8 Hz, 2H), 7.61 (s, 2H), 8.15 (d, *J* = 8 Hz, 2H). NIR/vis: λ_{abs}= 755 nm, λ_{em} = 773 nm, ε = 1.2 × 10^5 $M^{-1}cm^{-1}$ (pH < 5), λ_{abs}= 513 nm (pH > 5). Φ_F (MeOH): 0.084. ESI-MS, *m/z*: 701 (M^+ -Na + H, 100%).

Peptide synthesis and conjugation with pH-activatable dye 4 (6,7)

Cyclic RGD **6** was prepared as previously described (24). Conjugation of the peptide with dye was performed on solid supports. cRGD (**6**, 3.64 mg, 4 μmol), 2-(6-Chloro-1H-benzotriazole-1-yl)-1,1,3,3-tetramethylaminium hexafluorophosphate (HCTU, 1.7 mg, 4.1 μmol) and *N*-methylmorpholine (0.45 μL, 4.1 μmol) were added at room temperature to **4** (2.8 mg, 4 μmol) in 0.2 mL anhydrous DMSO. The vortexing continued for 1 h at RT in the dark, the reaction mixture was poured over 2 mL ice-cold water and purified by HPLC equipped with a C18 (22 × 250 mm, 10 μm) HPLC column. HPLC mobile phase was a mixture of solvent A = H_2O + 0.1% formic acid, and solvent B = CH_3CN + 0.1% formic acid at a flow rate of 12 mL/min. After lyophilization, the compound **7** was obtained as a green powder (2.88 mg, 45%).

Deprotection of 7

Compound **7** was dissolved in a 1 mL mixture of 95% trifluoroacetic acid (TFA), 2.5 % triisopropylsilane and 2.5% water. The solution was vortexed at RT for 2.5 h, dissolved the residues in 2 mL ice cold water, and purified the product by reverse phase HPLC as described above (retention time 23 min). After lyophilization, the dye-cRGD conjugate **8** (cyclo(Arg-Gly-Asp-D-Phe-Lys)-NH_2; 1.84 mg, 85%) was obtained as green powder. Yield 85%. MALDI-TOF MS *m/z* 1285 ($[M-Na + H]^+$, calcd 1285).

Spectral properties and pKa measurements

The absorption and emission spectra were determined using a spectrophotometer and fluorometer, respectively. The molar extinction coefficient was determined by Beer's law at low concentrations of 0.1–0.6 μM. The relative fluorescence quantum yield was determined by using the equation(30):

$$\Phi_{F(x)} = (A_s/A_x)\,(F_x/F_s)\,(n_x/n_s)^2\Phi_{F(s)}$$

where $\Phi_{F(X)}$ is the fluorescence quantum yield, *A* is the absorbance, *F* is the area under the emission curve, *n* is the refractive index of the solvents used in the measurement, and the subscripts *s* and *x* represent the standard and unknown, respectively. Indocyanine green (ICG) was used as a reference standard, which has the value of 0.078 in MeOH (31).

The spectral properties of NIR pH dye were determined in water, using a spectrophotometer for absorption and a fluorometer for fluorescence measurement. For pH titrations, dye **1** in water was acidified with dilute aq. HCl until the desired pH was obtained by titrating the solution with dilute aqueous NaOH with constant ionic strengths of 0.1 M. The pH of the solution was continuously measured with a pH meter. At each pH point, the absorption and fluorescence measurements were determined. The pKa value was calculated from the sigmoidal dose-response curve fit using GraphPad Prism 5.0 software.

Cell culture

4T1/*luc* breast cancer cells were purchased from Sibtech and MDA-MB-435 breast cancer cells were purchased from ATCC. Cells were maintained in humidified atmosphere containing 5% CO_2 at 37 °C in DMEM culture medium supplemented with 10% fetal calf serum, 100 units/ml penicillin and 100 units/ml streptomycin.

Tissue Homogenate Assays

Liver was dissected from rats after euthanasia and snap frozen. Frozen tissue was homogenized using a Bessman tissue pulverizer followed by addition of sterile saline. The pH of tissue homogenates were adjusted by addition of HCl to give pH ranges of 3–7. Tissue homogenate solutions were pippetted into 96-well microtiter plates. NIR pH-activatable dye **1** was dissolved in DMSO and added to homogenate wells and mixed for total volume of 0.25 mL per well and dye concentration of 10 μM. Fluorescence imaging was performed using the Pearl NIR fluorescence imaging system (LICOR Biosciences, Lincoln, NE) and eXplore Optix Time-domain diffuse optical imaging system (Advanced Research Technologies, Montreal, Canada). The Pearl imaging system acquires images in brightfield as well as excitation and emission at 685/710 nm and 785/810 nm, respectively. The eXplore Optix utilizes a 780 nm pulsed laser for excitation with emission detected at 830 nm using time-correlated single photon counting (TCSPC) for fluorescence intensity measurements.

Confocal microscopy of internalization of dye 8 into MDA-MB-435 and 4T1/*luc* cells

Cells were grown on LabTek microscope slides. Cells were treated for 1, 4, or 6 h with dye **8**. For lysosomal staining, 100 nM Lysotracker Green was added for the last 2 h of incubation. After treatment, cells were rinsed with PBS containing 1 mM $CaCl_2$, mounted with ProLongGold mounting medium (Invitrogen) and cover-slipped. The slides were imaged the next day using a 60x/1.20M, 0.13–0.21 NA water immersion objective as well as 488 nm and 633 nm lasers for excitation.

In vivo and ex vivo tumor imaging of breast cancer

All animal studies were performed in accordance with protocols approved by the Washington University School of Medicine Animal Studies Committee. Breast tumors were initiated in mice by injecting luciferase transfected mouse mammary carcinoma (4T1*luc*) cells either subcutaneously in 6-week old female NCR nude mice or orthotopically into the mammay fat pad in 6-week old female balb/c mice. After tumors had grown to 5–7 mm diameter, imaging studies were performed. The probe **8** was dissolved in DMSO then diluted with water for final concentration of 20 μM in 20% DMSO and 80% water. Probe **8** solution was injected intravenously via lateral tail vein (2 nmol/mouse, n =3). Fluorescence imaging was performed using the eXplore Optix TD-DOI system and the Pearl NIR imaging system at 1, 4, 6 and 24 h post injection. After the 24 h in vivo imaging time point, the mice were euthanized and organ tissues removed, placed on disposable petri dish and imaged as described above. Region of interest (ROI) analysis was performed using ImageJ image analysis software or Peral imaging software. Mean fluorescence intensities were measured for each tissue to assess biodistribution of probe **8**.

RESULTS AND DISCUSSION

Synthesis and spectral properties of pH-activatable NIR fluorophore

For efficient tumor imaging, the pH-sensitive dye should possess the following features: (1) minimal or no fluorescence in neutral to basic media but highly fluorescent in acidic media (pH < 7); (2) maximum excitation wavelength in the NIR region (λ_{max} > 700 nm); (3) good

water-solubility; and (4) functionalizable group for conjugation to biomolecules. Among many pH-sensitive fluorophores, NIR-absorbing norcyanines satisfy most of these criteria. The typical molecular framework of norcyanines has a pH-sensitive site on the heterocyclic ring due to the presence of one or more non-substituted nitrogen atoms. Previously, our group and others reported the syntheses and spectral properties of NIR pH-sensitive dyes (10,32). The limited water-solubility and lack of functionalizable groups for subsequent conjugation with biomolecules make these dyes less optimal for in vivo imaging. To overcome these drawbacks, we first developed a symmetrically-substituted water-soluble norcyanine dye **1**. Dye **1** (Figure 2a) exhibited characteristic pH-dependent spectral changes, with absorption maxima in the NIR window in acidic media. A hypsochromic shift to the visible region was observed in basic media to give **1′** with calculated pKa of 4.7 (Figure 2b & 2c).

This reversible, pH-dependent spectral shift arises from the protonation and deprotonation of the indolium ring nitrogen. The distinct characteristic alternation of π electronic charges that define a “polymethine state” (33) is lost during deprotonation process, which results in the hypsochromic shift of the absorption maxima of these dyes from NIR to visible wavelength. To further explore the behavior of probe in tissue homogenates, fluorescence imaging was performed using homogenized liver tissues. The pH of tissue homogenates was adjusted by adjusting tissue pH with HCl to give a range of 3–7. Expectedly, the fluorescence intensity of pH-activatable dye **1** at 800 nm was not detected at pH > 6, suggesting that the dye will have low background fluorescence in extracellular tissue (Figure 2d). In contrast, at pH < 6, bright fluorescence was observed. These data are in good agreement with the pKa value determined in aqueous solution. The results indicate fluorescence will be detected in acidic tissue compartments such as lysosomes.

Conjugation of pH-sensitive dye with a tumor-targeting cRGD for selective tumor imaging

For efficient tumor targeting and selective activation of pH probes in the lysosomes, dye **1** was conjugated to ABIR targeting RGD peptides. The RGD sequence has high affinity for ABIR, which is overexpressed by many tumor cells. In addition, binding of this peptide to ABIR results in receptor-medicated endocytosis and lysosomal accumulation of the molecular probe in cancer cells. Synthesis of the molecular probe was achieved by introducing carboxylic acid functionality to the NIR pH-sensitive dye **1**. Previously, we reported the synthesis of *meso*-phenylcarboxylic acid functionalized dye using a modified Suzuki-Miyaura method (34). However, attempts to incorporate free carboxy functionality using dye **1** failed to produce the desired dye **4**. The presence of unsubstituted heterocyclic nitrogen may promote a complex formation with palladium catalyst to give a dimeric isomer with absorption maxima in the visible range. Such compounds do not have apparent pH-dependent spectral properties. To overcome these drawbacks, Vilsmeier reagent **3** was first reacted with 4-carboxyphenyboronic acid under

Suzuki-coupling conditions to give the intermediate **5**. Further heating of **5** with indolium moiety **2** in basic medium finally gave the desired dye **4** as green solid.

Among many RGD peptides available to label the carboxy-functionalized fluorophore **4,** we chose cyclo(Arg-Gly-Asp-D-Phe-Lys)-NH_2 peptide. This peptide sequence includes an ABIR-targeting peptide motif as well as a free – NH_2 functionalizable group for conjugation to pH-sensitive dye **4**. Briefly, activation of carboxy-functionality of dye **4** with HCTU in *N*-methylmorpholine (NMM) followed by the reaction with lysine residue of the cyclic peptide **6** provides the dye-peptide conjugate **7**. Removal of protecting groups with TFA affords the desired targeting probe **8**.

Internalization Studies

Based on the pKa of the dye, selective accumulation of the probe in the late endosome or lysosome of tumor cells is necessary for fluorescence activation of the probe. Lysosomal uptake of pH-probe **8** in 4T1/*luc* and MDA-MB-435 cells was evaluated by co-staining with Lysotracker green, a lysosome selective stain at 1 h, 4 h and 6 h. Co-localization of pH-activatable probe **8** with Lysotracker and subsequent fluorescence amplification is evident in both cell lines, although higher accumulation of the probe was observed in MDA-MB-435. The cellular distribution of fluorescence was punctuate, as opposed to diffuse, which is consistent with fluorescence activation occurring in intracellular compartments such as the lysosomes and not in the cytosol. These data demonstrate the feasibility of using pH probe **8** for selective fluorescence activation in the target tumor lysosomes.

In vivo tumor imaging of breast cancer 4T1/*luc*

To evaluate the feasibility of imaging tumor with pH-activatable probe, we developed subcutaneous 4T1/*luc* tumor in mice. The tumors were developed on the flanks of rodents, a model frequently used in our lab with minimal metastasis. The localized tumor allows direct assessment of the new probe in this confined in vivo environment. Selective uptake of the ABIR-targeted pH-activatable probe **8** for in vivo tumor imaging is shown in Figure 4A. The accumulation in tumor and subsequent fluorescence activation of pH probe **8** is evident as early as 1 h post-injection (Figure 4B) and reached maximum contrast by 4 h post-injection (Figure 4C).

In vivo and ex vivo tumor imaging of orthotopic breast cancer 4T1/*luc*

Orthotopic tumor models closely resemble the biological environment of human tumors compared to subcutaneous xenografts models. To demonstrate the versatility of the pH probe **8** in imaging orthotopic tumor models and validate the selective amplification fluorescence in acidic compartment of tumor cells, we administered **8** to mice with orthotopic syngeneic breast tumors. In vivo fluorescence imaging results are shown in Figure 5. Immediately after injection, fluorescence signal was equivalent to pre-injection signal but increased with time. Fluorescence intensity increased in the tumor and liver regions, indicating uptake of **8** in tumor cells and hepatocytes, respectively. The fluorescence intensity in the tumor region was high at 4 h after injection and remained high for up to 24 h post-injection. Based on previous studies with NIR dye-labeled cRGD peptides, uptake of the probe in the tumor cells is mediated by ABIR-endocytosis. As shown by the cell microscopy study, the observed fluorescence amplification is attributed to delivery of the probe to the lysosomes, which is more acidic than other cellular organelles. The increase in fluorescence is time-dependent and correlates with the trafficking of the probe from the early endosomes, through late endosomes to the lysosomes. This pathway corresponds to increase in intracellular acidity of the organelles. The liver is the primary excretion organ for this molecular probe, which is probably acidified in the process of hepatobiliary excretion pathway. Fluorescence intensity increased to a lesser extent in other organs, reflecting the expression of ABIR in other tissues than the tumor.

The high tumor-specific contrast was confirmed by ex vivo tissue imaging (Figure 6A). Region of interest (ROI) analysis of ex vivo tissue fluorescence confirmed the tumor fluorescence signal enhancement observed in vivo (Figure 6B). Ex-vivo fluorescence images of organ tissues show an excellent tumor-to-muscle ratio with an average value of 11:1 (tumor : muscle). High fluorescence was also detected in the kidneys and liver, indicating a mixed route of elimination from the body. Interestingly, tumor metastases (~ 1 mm) were detected in the lungs of one mouse by fluorescence imaging (Figure 6A), which was further confirmed by histological analysis (Figure 6C). It is well established that 4T1/*luc* tumors exhibit high metastastatic spread to lungs (35). The high fluorescence detected in these small

tumor nodules further demonstrates the capability of detecting tumors in their natural environments due to the pH enhanced contrast mechanism.

CONCLUSION

We have developed ABIR-targeting NIR pH-activatable probe for in vivo imaging applications with high tumor selectivity. This pH-activatable probe offer several advantages over other NIR probes. First, NIR pH-sensitive probes are ideal for in vivo applications due to low background signal. Second, selective accumulation and subsequent fluorescence activation of pH-activatable probe in tumor lysosomes offers improved specificity with high fluorescence signal from tumor compared to non-target tissues. The results of in vitro and in vivo studies demonstrate the potential imaging applications of NIR pH-activatable probes for primary and metastatic tumor detection with high sensitivity and specificity.

Acknowledgments

This study was supported in part by the US National Institutes of Health NIBIB grants R01 EB007276, EB008111, EB 008458 and NCI R33 CA123537.

LITERATURE CITED

1. Kaijzel EL, van Heijningen PM, Wielopolski PA, Vermeij M, Koning GA, van Cappellen WA, Que I, Chan A, Dijkstra J, Ramnath NW, Hawinkels LJ, Bernsen MR, Lowik CW, Essers J. Multimodality imaging reveals a gradual increase in matrix metalloproteinase activity at aneurysmal lesions in live fibulin-4 mice. Circ Cardiovasc Imaging. 3:567–77. [PubMed: 20592247]
2. Kim DE, Kim JY, Schellingerhout D, Shon SM, Jeong SW, Kim EJ, Kim WK. Molecular imaging of cathepsin B proteolytic enzyme activity reflects the inflammatory component of atherosclerotic pathology and can quantitatively demonstrate the antiatherosclerotic therapeutic effects of atorvastatin and glucosamine. Mol Imaging. 2009; 8:291–301. [PubMed: 19796606]
3. Sheth RA, Upadhyay R, Stangenberg L, Sheth R, Weissleder R, Mahmood U. Improved detection of ovarian cancer metastases by intraoperative quantitative fluorescence protease imaging in a pre-clinical model. Gynecol Oncol. 2009; 112:616–22. [PubMed: 19135233]
4. Jaffer FA, Vinegoni C, John MC, Aikawa E, Gold HK, Finn AV, Ntziachristos V, Libby P, Weissleder R. Real-time catheter molecular sensing of inflammation in proteolytically active atherosclerosis. Circulation. 2008; 118:1802–9. [PubMed: 18852366]
5. Jaffer FA, Kim DE, Quinti L, Tung CH, Aikawa E, Pande AN, Kohler RH, Shi GP, Libby P, Weissleder R. Optical visualization of cathepsin K activity in atherosclerosis with a novel, protease-activatable fluorescence sensor. Circulation. 2007; 115:2292–8. [PubMed: 17420353]
6. Barnett EM, Zhang X, Maxwell D, Chang Q, Piwnica-Worms D. Single-cell imaging of retinal ganglion cell apoptosis with a cell-penetrating, activatable peptide probe in an in vivo glaucoma model. Proc Natl Acad Sci U S A. 2009; 106:9391–6. [PubMed: 19458250]
7. Klohs J, Baeva N, Steinbrink J, Bourayou R, Boettcher C, Royl G, Megow D, Dirnagl U, Priller J, Wunder A. In vivo near-infrared fluorescence imaging of matrix metalloproteinase activity after cerebral ischemia. J Cereb Blood Flow Metab. 2009; 29:1284–92. [PubMed: 19417756]
8. Maxwell D, Chang Q, Zhang X, Barnett EM, Piwnica-Worms D. An improved cell-penetrating, caspase-activatable, near-infrared fluorescent peptide for apoptosis imaging. Bioconjug Chem. 2009; 20:702–9. [PubMed: 19331388]
9. Hilderbrand SA, Kelly KA, Niedre M, Weissleder R. Near infrared fluorescence-based bacteriophage particles for ratiometric pH imaging. Bioconjug Chem. 2008; 19:1635–9. [PubMed: 18666791]
10. Hilderbrand SA, Weissleder R. Optimized pH-responsive cyanine fluorochromes for detection of acidic environments. Chem Commun (Camb). 2007:2747–9. [PubMed: 17594041]

11. Urano Y, Asanuma D, Hama Y, Koyama Y, Barrett T, Kamiya M, Nagano T, Watanabe T, Hasegawa A, Choyke PL, Kobayashi H. Selective molecular imaging of viable cancer cells with pH-activatable fluorescence probes. Nat Med. 2009; 15:104–9. [PubMed: 19029979]
12. Ogawa M, Kosaka N, Regino CA, Mitsunaga M, Choyke PL, Kobayashi H. High sensitivity detection of cancer in vivo using a dual-controlled activation fluorescent imaging probe based on H-dimer formation and pH activation. Mol Biosyst. 6:888–93. [PubMed: 20567775]
13. Panizzi P, Nahrendorf M, Wildgruber M, Waterman P, Figueiredo JL, Aikawa E, McCarthy J, Weissleder R, Hilderbrand SA. Oxazine conjugated nanoparticle detects in vivo hypochlorous acid and peroxynitrite generation. J Am Chem Soc. 2009; 131:15739–44. [PubMed: 19817443]
14. Hilderbrand SA, Weissleder R. Near-infrared fluorescence: application to in vivo molecular imaging. Curr Opin Chem Biol. 14:71–9. [PubMed: 19879798]
15. Lee H, Akers WJ, Cheney PP, Edwards WB, Liang K, Culver JP, Achilefu S. Complementary optical and nuclear imaging of caspase-3 activity using combined activatable and radio-labeled multimodality molecular probe. J Biomed Opt. 2009; 14:040507. [PubMed: 19725712]
16. Levi J, Kothapalli SR, Ma TJ, Hartman K, Khuri-Yakub BT, Gambhir SS. Design, synthesis, and imaging of an activatable photoacoustic probe. J Am Chem Soc. 132:11264–9. [PubMed: 20698693]
17. Mieog JS, Hutteman M, van der Vorst JR, Kuppen PJ, Que I, Dijkstra J, Kaijzel EL, Prins F, Lowik CW, Smit VT, van de Velde CJ, Vahrmeijer AL. Image-guided tumor resection using real-time near-infrared fluorescence in a syngeneic rat model of primary breast cancer. Breast Cancer Res Treat.
18. Salthouse CD, Reynolds F, Tam JM, Josephson L, Mahmood U. Quantitative Measurement of Protease-Activity with Correction of Probe Delivery and Tissue Absorption Effects. Sens Actuators B Chem. 2009; 138:591–597. [PubMed: 20161242]
19. Mu CJ, Lavan DA, Langer RS, Zetter BR. Self-assembled gold nanoparticle molecular probes for detecting proteolytic activity in vivo. ACS Nano. 4:1511–20. [PubMed: 20146506]
20. Elias DR, Thorek DL, Chen AK, Czupryna J, Tsourkas A. In vivo imaging of cancer biomarkers using activatable molecular probes. Cancer Biomark. 2008; 4:287–305. [PubMed: 19126958]
21. Kamiya M, Kobayashi H, Hama Y, Koyama Y, Bernardo M, Nagano T, Choyke PL, Urano Y. An enzymatically activated fluorescence probe for targeted tumor imaging. J Am Chem Soc. 2007; 129:3918–29. [PubMed: 17352471]
22. Zhang X, Lin Y, Gillies RJ. Tumor pH and its measurement. J Nucl Med. 51:1167–70. [PubMed: 20660380]
23. Cardone RA, Casavola V, Reshkin SJ. The role of disturbed pH dynamics and the Na+/H+ exchanger in metastasis. Nat Rev Cancer. 2005; 5:786–95. [PubMed: 16175178]
24. Ye Y, Bloch S, Xu B, Achilefu S. Novel near-infrared fluorescent integrin-targeted DFO analogue. Bioconjug Chem. 2008; 19:225–34. [PubMed: 18038965]
25. Eliceiri BP, Cheresh DA. Role of alpha v integrins during angiogenesis. Cancer J. 2000; 6(Suppl 3):S245–9. [PubMed: 10874494]
26. Ria R, Vacca A, Ribatti D, Di Raimondo F, Merchionne F, Dammacco F. Alpha(v)beta(3) integrin engagement enhances cell invasiveness in human multiple myeloma. Haematologica. 2002; 87:836–45. [PubMed: 12161360]
27. Meyer A, Auernheimer J, Modlinger A, Kessler H. Targeting RGD recognizing integrins: drug development, biomaterial research, tumor imaging and targeting. Curr Pharm Des. 2006; 12:2723–47. [PubMed: 16918408]
28. Mason, JC. Chemistry. Georgia State University; Atlanta: 2001. p. 1-202.
29. Lee H, Mason JC, Achilefu S. Synthesis and spectral properties of near-infrared aminophenyl-, hydroxyphenyl-, and phenyl-substituted heptamethine cyanines. J Org Chem. 2008; 73:723–5. [PubMed: 18095702]
30. Demas JN, Crosby GA. Measurement of photoluminescence quantum yields. Review. J phys Chem. 1971; 75:991–1023.
31. Benson RC, Kues HA. Fluorescence properties of indocyanine green as related to angiography. Phys Med Biol. 1978; 23:159–63. [PubMed: 635011]

32. Zhang Z, Achilefu S. Design, synthesis and evaluation of near-infrared fluorescent pH indicators in a physiologically relevant range. Chem Commun (Camb). 2005:5887–9. [PubMed: 16317464]

33. Tyutyulkov, NFJ.; Mehlhorn, A.; Dietz, F.; Tadjer, A. Polymethine Dyes: Structure and Properties. St. Kliment Ohridski University Press; Sofia, Bulgaria: 1991.

34. Lee H, Mason JC, Achilefu S. Heptamethine cyanine dyes with a robust C-C bond at the central position of the chromophore. J Org Chem. 2006; 71:7862–5. [PubMed: 16995699]

35. Hiraga T, Hata K, Ikeda F, Kitagaki J, Fujimoto-Ouchi K, Tanaka Y, Yoneda T. Preferential inhibition of bone metastases by 5′-deoxy-5-fluorouridine and capecitabine in the 4T1/luc mouse breast cancer model. Oncol Rep. 2005; 14:695–9. [PubMed: 16077977]

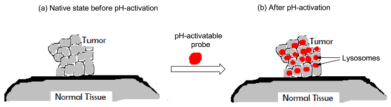

Figure 1.

Selective pH-activation of tumor in acidic lysosomal compartments. (a) Tumor in native state before pH-activation and (b) selective activation of pH probe in lysosomal compartment of tumor cells with minimal fluorescence in non-lysosomal compartments of tumor cells and normal (non-target) tissue.

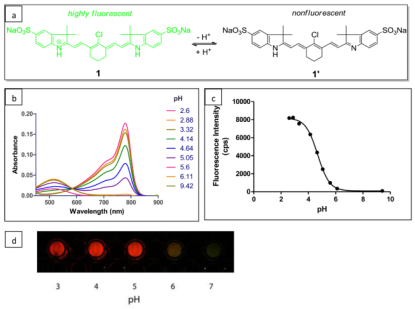

Figure 2.

(***a***) Structure of pH-sensitive dye **1** in acidic and basic media. The reversible pH-sensitivity of dye **1** arises from the protonation-deprotonation of indolium nitrogen atom (***b***) pH-dependent absorption spectral changes at pH range of 2.6–9.4 (***c***) pH response of dye **1** using fluorescence intensity at 795 nm to give pKa of 4.7 (***d***) fluorescence intensity change of dye **1** in liver tissue homogenate at pH range of 3–7.

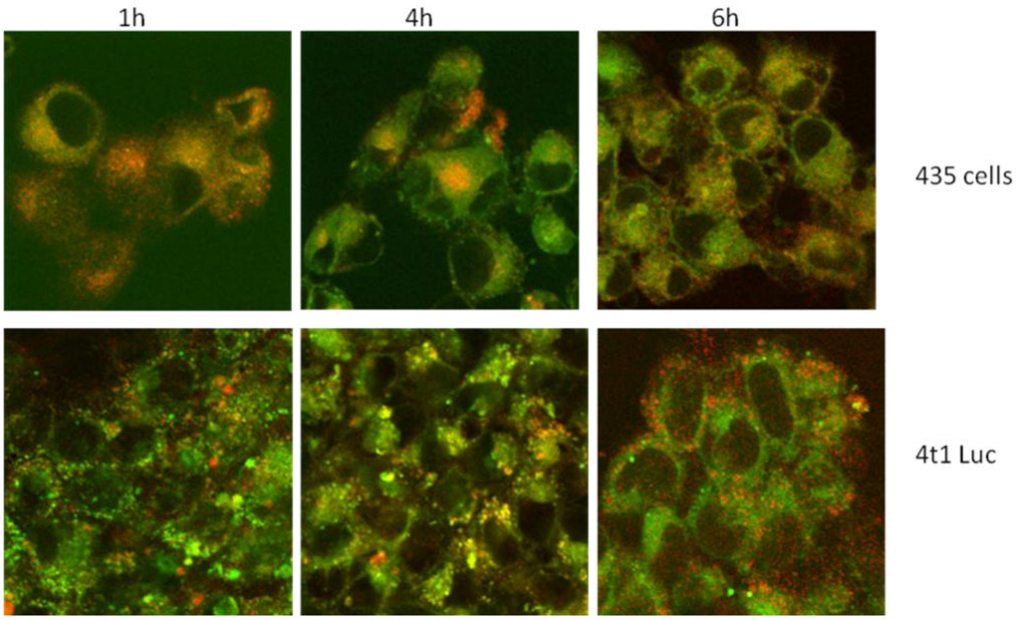

Figure 3.
Lysosomal accumulation with MDA-MB-435 cells or 4T1 *luc* cells after incubation with **8** at 1, 4, and 6 h. When Dye8 (red) overlaps with the lysosomal stain (green) the resulting image is orange. The punctuate distribution of fluorescence is consistent with fluorescence activation occurring in the lysosomes.

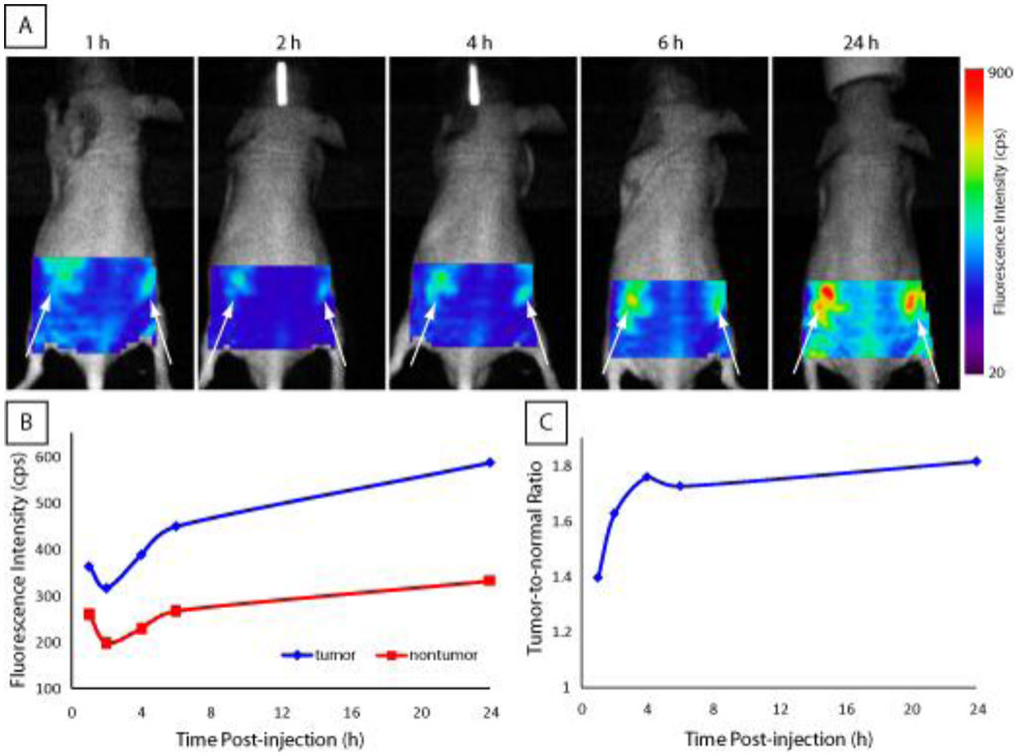

Figure 4.

(A) Fluorescence image of LS 573 in 4T1/*luc* tumor-bearing mouse at indicated times after intravenous administration. Arrows indicate bilateral subcutaneous tumor locations. (B) Plot of average fluorescence intensity values for tumor regions compared with non-tumor control region selected *in vivo* imaging data. (C) Plot of *in vivo* tumor contrast at each timepoint showing that high contrast was achieved by 4 h and was maintained for at least 24 h post-injection.

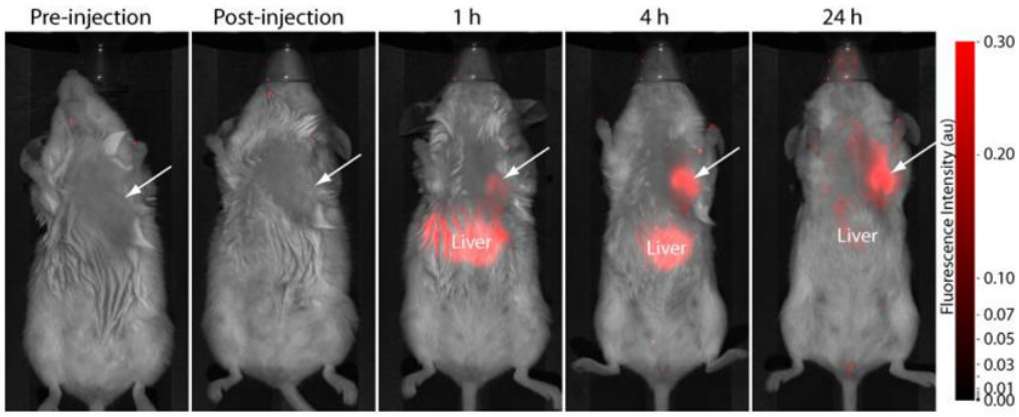

Figure 5.

Fluorescence images of NIR pH-activatable probe **8** in orthotopic 4T1/*luc* tumor-bearing mice at various time points. Fluorescence intensity in the tumor region (arrow) increased with time relative to non-tumor areas, reaching a plateau by 24 h.

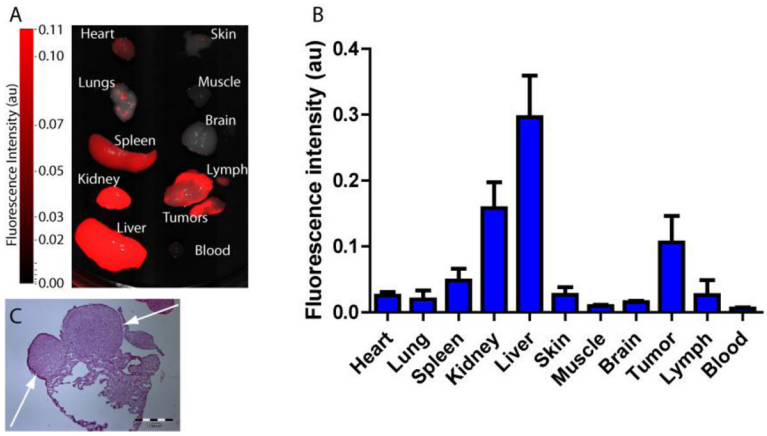

Figure 6.

(A) Ex vivo fluorescence biodistribution image of **8** in organ tissues from 4T1/*luc* orthotopic tumor bearing mice at 24 h post-injection *(B)* Fluorescence intensity data from ROI analysis of organ tissues *(C)* Histologic confirmation of ~ 1 mm tumor metastases (arrow) in the lungs. Metastases to the lymph nodes was not confirmed.

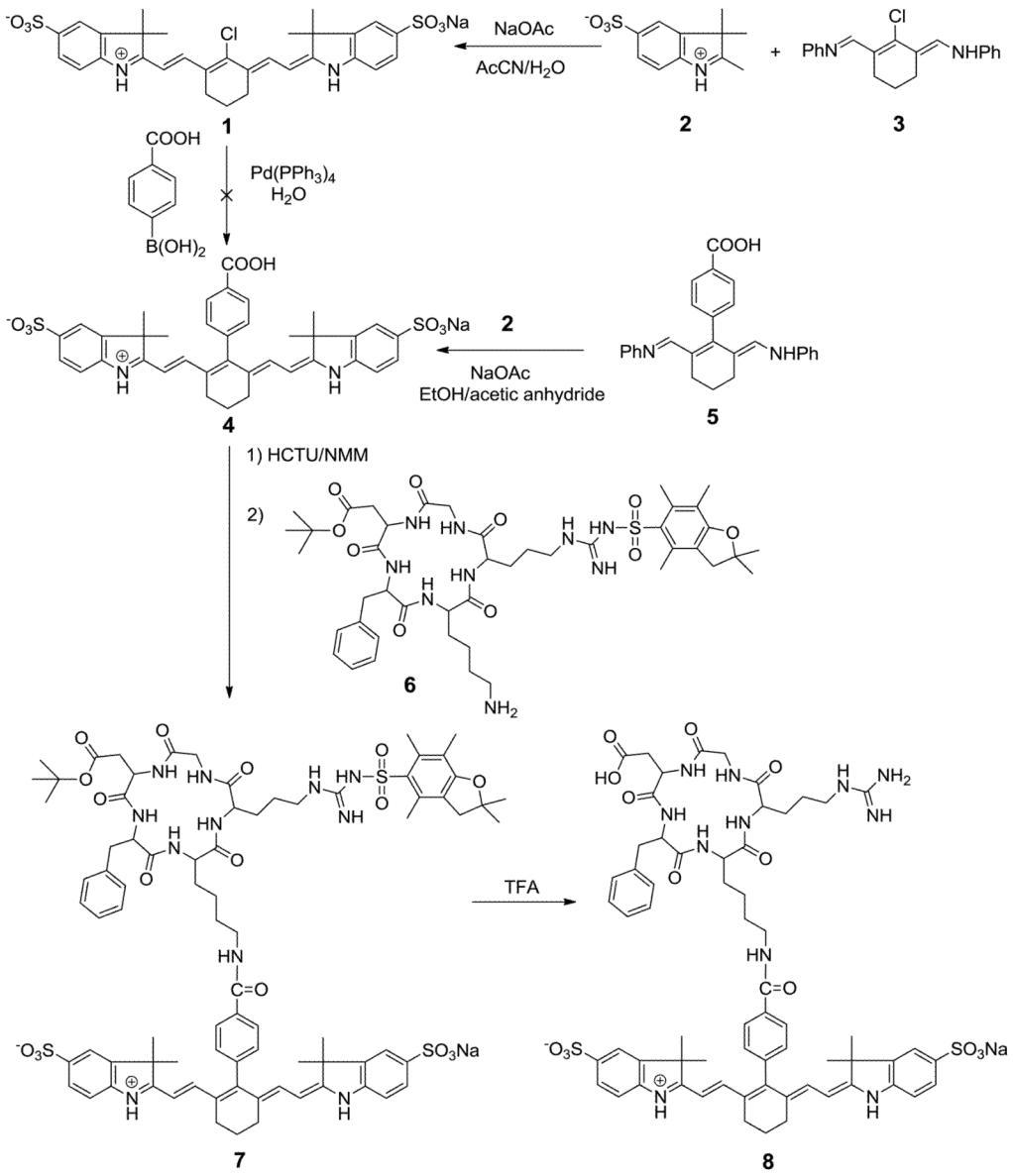

Scheme 1.
Synthetic route to $\alpha_v\beta_3$-targeting pH-sensitive dye 8.